

# Magnons in the half-doped manganites

C. I. Ventura and B. Alascio

*Centro Atómico Bariloche, 8400-Bariloche, Argentina.*

Recently, based on the refined crystal structure of  $\text{Pr}_{0.6}\text{Ca}_{0.4}\text{MnO}_3$  from neutron diffraction, Daoud-Aladine et al. [Phys.Rev.Lett.**89**,97205(2002)] have proposed a new ground state structure for the half-doped manganites  $\text{R}_{0.5}\text{Ca}_{0.5}\text{MnO}_3$ , where R is a trivalent ion like Bi, La, Pr, Sm or Y. Their proposal describes the CE magnetic structure attributed to these materials as an arrangement of dimers along the ferromagnetic Mn zig-zag chains that form it. The formation of dimers is in accordance with previous theoretical calculations based on simplified models for these compounds. However, the dimers' proposal is in conflict with the Goodenough-Kanamori-Anderson rules, which give a coherent description of many transition metal insulating compounds and predict the coexistence of  $\text{Mn}^{3+}$  and  $\text{Mn}^{4+}$  ions in equal parts in the half-doped manganites. On the other hand, Rivadulla et al. [Phys.Rev.B **66**,174432(2002)] have studied several single crystal samples of half-doped manganites and propose a phase diagram in terms of the tolerance factor which contains both types of structures. In the present work we have calculated the magnon dispersion relations for the CE magnetic structure, arising for each type of proposal: the charge ordered and the dimer phases, respectively. We consider a three-dimensional unit cell containing 16 spins, and compare the magnetic excitations along different paths in the first Brillouin zone. We conclude that measurement of the magnon dispersion relations should allow a clear distinction between the two proposals, predicting qualitative differences arising along specific directions of propagation in the first Brillouin zone.

75.25.+z,75.50.-y,75.47.-m

Half-doped manganites of stoichiometry  $\text{R}_{1-x}\text{Ca}_x\text{MnO}_3$ ,  $x=1/2$ , where R is a trivalent ion like Bi, La, Pr, Sm or Y, display a rich phase diagram depending on their composition<sup>1</sup>: in the absence of magnetic field, charge-ordered antiferromagnetic insulator phases (COA), ferromagnetic metallic (FM), antiferromagnetic insulator, and paramagnetic phases have been reported. Strong colossal magnetoresistance appears by driving the materials from COA to FM by application of moderate external magnetic fields.

Below the Néel temperature the half-doped compounds are found in the CE magnetic structure<sup>2</sup>, in which ferromagnetic Mn zig-zag chains contained in parallel planes are found in an antiferromagnetic arrangement. The description of the CE magnetic structure found in most half-doped manganites is based on the well known Goodenough-Kanamori-Anderson (GKA) rules<sup>3</sup>, implying a checkerboard ordering of  $\text{Mn}^{3+}/\text{Mn}^{4+}$  ions in the crystal<sup>4</sup>, as shown in Fig.1.

(+orbital) ordered (CO) scenario for half-doped manganites in

However, Daoud-Aladine et al.<sup>5</sup> have shown recently that the crystal structures of  $\text{Pr}_{0.60}\text{Ca}_{0.40}\text{MnO}_3$  single crystals obtained from neutron diffraction data can not be interpreted in terms of  $\text{Mn}^{3+}/\text{Mn}^{4+}$  charge ordering. Rather, the data suggest an intermediate valence of 3.5 for all Mn ions. Furthermore, the XANES results on the Mn K-edge of  $\text{La}_{0.50}\text{Ca}_{0.50}\text{MnO}_3$  by J.García et al.<sup>6</sup> suggest also the same valence for Mn. On the basis of these results, Daoud-Aladine et al. propose that the zig-zag ferromagnetic chains contained in the CE magnetic structure are formed by a succession of Mn dimers (or Zener polarons)<sup>5</sup>, such as indicated in Fig.2. Mn ions forming the dimers share one electron and point in the same direction forming a large spin unit. The chains order antiferromagnetically between them within the Mn structure. Theoretically, such situation had been studied previously in one<sup>7</sup>, two<sup>8</sup> and three dimensional<sup>9</sup> structures as a consequence of the competition between double exchange and superexchange.

More recently, Rivadulla et al.<sup>10</sup> have proposed a new phase diagram for the half-doped manganites in terms of the tolerance factor  $t$ . In the new phase diagram both phases appear: the charge ordered phase is found for  $t$  below a critical value  $t_c = 0.975$ , and the dimer phase for  $t$  larger than  $t_c$ . Both (insulating) phases are separated by a unique (metallic) ferromagnetic phase. Contrary to the usual metallic ferromagnetic phase of hole doped manganites which is stabilized by pressure, the ferromagnetic phase that separates the two insulating phases at half filling can be suppressed by pressure.

Since both insulating phases proposed for the CE magnetic structure, the charge ordered and the dimer one, have some common characteristics like: their insulating character, both are metamagnetic going into a metallic ferromagnetic phase under moderate magnetic fields, include zig-zag ferromagnetic chains, etc., we decided to calculate their magnetic excitation spectra as a mean to distinguish between them, and also as a way to check the difference of the magnetic interaction along the chains in the proposed models.

Therefore, we have considered a basic three-dimensional unit cell containing 16 spins (Mn), half of them in each of two consecutive planes, as shown in Fig. 3. For the charge ordered phase, two different values of spin (representing

the  $S_1 = 2$  and  $S_2 = 3/2$  spins of  $\text{Mn}^{3+}$  and  $\text{Mn}^{4+}$ , respectively) would appear, in checkerboard arrangement like shown in Fig. 1. The interactions are superexchange couplings between all Mn ions: one ferromagnetic coupling along nearest neighbour spins on a chain ( $F'=F$ ), and two antiferromagnetic nearest neighbour couplings: one inter-chain coupling ( $A$ ) and one inter-plane ( $A'$ ). On the other hand, for the dimer phase, only one value of spin ( $S_1 = S_2$ ) would be present, while the ferromagnetic coupling between nearest neighbour spins along a zig-zag chain now would take two different values: the interaction between the spins forming a dimer is double exchange ( $F'$ ), while a superexchange interaction ( $F$ ) couples nearest neighbour spins in different dimers.

This state of things can be described by a model composed of a series of appropriate nearest neighbour Heisenberg coupling terms. With the notation for magnetic couplings introduced in Fig. 3, the following Hamiltonian has been considered:

$$\begin{aligned}
H = & -F' \sum_{(n,\alpha;n',\alpha')/ \in D} \mathbf{S}_{n,\alpha} \cdot \mathbf{S}_{n',\alpha'} - F \sum_{(n,\alpha;n',\alpha')/ NN, \in C, \notin D} \mathbf{S}_{n,\alpha} \cdot \mathbf{S}_{n',\alpha'} \\
& + A \sum_{(n,\alpha;n',\alpha')/ NN, \notin C, \in P} \mathbf{S}_{n,\alpha} \cdot \mathbf{S}_{n',\alpha'} + A' \sum_{(n,\alpha;n',\alpha')/ NN, \notin P} \mathbf{S}_{n,\alpha} \cdot \mathbf{S}_{n',\alpha'} . \quad (1)
\end{aligned}$$

We have identified the position of the spins by indices:  $\alpha = (i, j, k)$  to locate the 3D unit cell in the Bravais lattice, and site labels  $n (= 1, \dots, 16)$  to distinguish the spins inside one unit cell. Capital letters  $D$  denote a dimer,  $NN$  nearest neighbour sites,  $C$  one chain, and  $P$  one plane.  $F, F', A$  and  $A'$  are positive. For the charge-ordered phase the ferromagnetic couplings along a zig-zag chain are  $F'=F$ , while each coupling term will include spins of different magnitude (due to the checkerboard arrangement shown in Fig. 1).

To calculate the magnetic excitations at low temperatures we have used the Holstein-Primakoff transformation in linear spin wave approximation<sup>11</sup>, which in our case demanded the introduction of 16 different kinds of boson operators, one for each spin inside the unit cell of Fig. 3, distinguishing the spin-up and spin-down sublattices. That is, we introduced for the spin-up sublattice:

$$\begin{aligned}
S_{n,\alpha}^+ &= \sqrt{2S_n} a_{n,\alpha} \\
S_{n,\alpha}^- &= \sqrt{2S_n} a_{n,\alpha}^\dagger \\
S_{n,\alpha}^z &= S_n - a_{n,\alpha}^\dagger a_{n,\alpha} , \quad (2)
\end{aligned}$$

where  $n = 1, 2, 3, 4, 13, 14, 15, 16$  with the notation of Fig.3, and  $S_n$  is the magnitude of spin  $n$ . Without loss of generality, we can put:  $S_n = S_1$ , for  $n = 1, 3, 14, 16$ , and  $S_n = S_2$ , for  $n = 2, 4, 13, 15$  ( $S_1 = S_2$ , for the dimer phase).

Similarly for the spin-down sublattice, we introduced:

$$\begin{aligned}
S_{n,\alpha}^+ &= \sqrt{2S_n} b_{n,\alpha}^\dagger \\
S_{n,\alpha}^- &= \sqrt{2S_n} b_{n,\alpha} \\
S_{n,\alpha}^z &= -S_n + b_{n,\alpha}^\dagger b_{n,\alpha} , \quad (3)
\end{aligned}$$

where  $n = 5, 6, 7, 8, 9, 10, 11, 12$  with the notation of Fig.3. Without loss of generality, we put:  $S_n = S_1$ , for  $n = 5, 7, 10, 12$ , and  $S_n = S_2$ , for  $n = 6, 8, 9, 11$ .

Introducing the Fourier transform of the boson operators (which for compactness we will denote here:  $a_{n,\vec{k}}^{(\dagger)} \equiv a_n^{(\dagger)}$ ;  $b_{n,\vec{k}}^{(\dagger)} \equiv b_n^{(\dagger)}$ ), we then determined the Hamiltonian, which for the dimer phase ( $S_1 = S_2 \equiv S$ ) takes the following form:

$$\begin{aligned}
H = & [F' + F + 2(A + A')] \left[ -8S^2N + S \left( \sum_{\vec{k}; n=1-4, 13-16} a_n^\dagger a_n + \sum_{\vec{k}; n=5-12} b_n^\dagger b_n \right) \right] \\
& - SF' \sum_{\vec{k}} \left[ a_2^\dagger a_3 + b_5^\dagger b_6 + b_{10}^\dagger b_{11} + a_{13}^\dagger a_{14} + e^{ik_x a_x} a_1^\dagger a_4 + e^{ik_y a_y} a_{15}^\dagger a_{16} + e^{-ik_y a_y} b_7^\dagger b_8 + e^{-ik_x a_x} b_9^\dagger b_{12} + H.c. \right] \\
& - SF \sum_{\vec{k}} \left[ a_1^\dagger a_2 + a_3^\dagger a_4 + a_{14}^\dagger a_{15} + b_6^\dagger b_7 + b_9^\dagger b_{10} + b_{11}^\dagger b_{12} + e^{-i(k_x a_x + k_y a_y)} b_5^\dagger b_8 + e^{i(k_x a_x + k_y a_y)} a_{13}^\dagger a_{16} + H.c. \right] \\
& + SA \sum_{\vec{k}} \left[ a_1 b_6 + a_3 b_6 + a_3 b_8 + b_7 a_4 + b_9 a_{14} + b_{11} a_{14} + b_{11} a_{16} + a_{15} b_{12} + e^{-ik_x a_x} a_1 b_8 + e^{-ik_x a_x} a_{13} b_{12} + \right. \\
& \quad \left. e^{-ik_y a_y} a_{13} b_{10} + e^{-ik_y a_y} a_{15} b_{10} + e^{ik_x a_x} b_5 a_4 + e^{ik_y a_y} b_5 a_2 + e^{ik_y a_y} b_7 a_2 + e^{ik_x a_x} b_9 a_{16} + H.c. \right] \\
& + SA' \sum_{\vec{k}} \left[ (1 + e^{-ik_z a_z}) (a_1 b_9 + a_2 b_{10} + a_3 b_{11} + a_4 b_{12}) + (1 + e^{ik_z a_z}) (b_5 a_{13} + b_6 a_{14} + b_7 a_{15} + b_8 a_{16}) + H.c. \right] , \quad (4)
\end{aligned}$$

where  $N$  denotes the total number of 16-spin unit cells as in Fig.3.

A similar expression can be written for the Hamiltonian of the charge-ordered phase, taking into account the two values of spin which will appear ( $S_1 \neq S_2$ ) and  $F = F'$  for that case.

The magnon excitations of the system for the dimer and the CO phases can then be obtained by diagonalization of the corresponding Hamiltonian. Concretely, we can obtain them by diagonalization of the following 16x16 general matrix (multiplied by  $S \equiv \sqrt{S_1 S_2}$ ), which for appropriate values of its parameters (as mentioned above) describes the two phases as particular cases:

$$\begin{pmatrix} \lambda_1 & -F & 0 & -F'\Phi_x & 0 & A & 0 & A\Phi_x & A'\theta_z & 0 & 0 & 0 & 0 & 0 & 0 & 0 \\ -F & \lambda_2 & -F' & 0 & A\Phi_y^* & 0 & A\Phi_y^* & 0 & 0 & A'\theta_z & 0 & 0 & 0 & 0 & 0 & 0 \\ 0 & -F' & \lambda_1 & -F & 0 & A & 0 & A & 0 & 0 & A'\theta_z & 0 & 0 & 0 & 0 & 0 \\ -F'\Phi_x^* & 0 & -F & \lambda_2 & A\Phi_x^* & 0 & A & 0 & 0 & 0 & A'\theta_z & 0 & 0 & 0 & 0 & 0 \\ 0 & -A\Phi_y & 0 & -A\Phi_x & -\lambda_1 & F' & 0 & F\Phi_x\Phi_y & 0 & 0 & 0 & 0 & -A'\theta_z & 0 & 0 & 0 \\ -A & 0 & -A & 0 & F' & -\lambda_2 & F & 0 & 0 & 0 & 0 & 0 & 0 & -A'\theta_z & 0 & 0 \\ 0 & -A\Phi_y & 0 & -A & 0 & F & -\lambda_1 & F'\Phi_y & 0 & 0 & 0 & 0 & 0 & 0 & -A'\theta_z & 0 \\ -A\Phi_x^* & 0 & -A & 0 & F\Phi_x^*\Phi_y^* & 0 & F'\Phi_y^* & -\lambda_2 & 0 & 0 & 0 & 0 & 0 & 0 & 0 & -A'\theta_z \\ -A'\theta_z^* & 0 & 0 & 0 & 0 & 0 & 0 & 0 & -\lambda_2 & F & 0 & F'\Phi_x & 0 & -A & 0 & -A\Phi_x \\ 0 & -A'\theta_z^* & 0 & 0 & 0 & 0 & 0 & 0 & F & -\lambda_1 & F' & 0 & -A\Phi_y^* & 0 & -A\Phi_y^* & 0 \\ 0 & 0 & -A'\theta_z^* & 0 & 0 & 0 & 0 & 0 & 0 & F' & -\lambda_2 & F & 0 & -A & 0 & -A \\ 0 & 0 & 0 & -A'\theta_z^* & 0 & 0 & 0 & 0 & F'\Phi_x^* & 0 & F & -\lambda_1 & -A\Phi_x^* & 0 & -A & 0 \\ 0 & 0 & 0 & 0 & A'\theta_z^* & 0 & 0 & 0 & 0 & A\Phi_y & 0 & A\Phi_x & \lambda_2 & -F' & 0 & -F\Phi_x\Phi_y \\ 0 & 0 & 0 & 0 & 0 & A'\theta_z^* & 0 & 0 & A & 0 & A & 0 & -F' & \lambda_1 & -F & 0 \\ 0 & 0 & 0 & 0 & 0 & 0 & A'\theta_z^* & 0 & 0 & A\Phi_y & 0 & A & 0 & -F & \lambda_2 & -F'\Phi_y \\ 0 & 0 & 0 & 0 & 0 & 0 & 0 & A'\theta_z^* & A\Phi_x^* & 0 & A & 0 & -F\Phi_x^*\Phi_y^* & 0 & -F'\Phi_y^* & \lambda_1 \end{pmatrix} \quad (5)$$

where the matrix columns (or rows) are related to the 16 boson operators, arranged in increasing order of their site label, and we have used the following notation for the matrix elements:  $\lambda_1 = S_2[F + F' + 2(A + A')]/S$ ;  $\lambda_2 = S_1[F + F' + 2(A + A')]/S$ ;  $\Phi_\alpha = \exp(ik_\alpha a_\alpha)$ , ( $\alpha = x, y$ );  $\theta_z = (1 + \exp(ik_z a_z))$ .

In Fig. 4 we exhibit our result for the 16 magnon excitation branches of the charge ordered (CO) phase, plotted along 8 different paths throughout the first Brillouin zone, using a typical set of relative values for the exchange coupling parameters for the system (in the present work we take the interdimer exchange coupling  $F$  as the energy unit, setting the overall energy scale) and a ratio of spin values  $S_1/S_2 = 1.3$ , such as that for  $\text{Mn}^{3+}/\text{Mn}^{4+}$  magnetic moments. The trajectories along the first Brillouin zone depicted extend between the following points:  $\Gamma \equiv 0 = (0, 0, 0)$ ,  $X = (\pi/a_x, 0, 0)$ ,  $Y = (0, \pi/a_y, 0)$ ,  $Z = (0, 0, \pi/a_z)$ ,  $M = (\pi/a_x, \pi/a_y, 0)$  and  $L = (\pi/a_x, \pi/a_y, \pi/a_z)$ .

In Fig. 5 we exhibit the results calculated for the magnons corresponding to the dimer phase, along the same first Brillouin zone trajectories. We have now considered:  $S_1/S_2 = 1$ ,  $F' = 2F$ , and the rest of the parameters unchanged for the sake of simplifying the comparison with the CO magnons. We have verified that the same magnon excitations are obtained for this phase, if one chooses a different relative array of the dimers on neighbour zig-zag chains.

Comparison of Figs. 4 and 5 reveals that a qualitative difference in the magnon branches predicted for the CO and the dimer phases can be clearly pointed out. Namely, that along the  $\Gamma \rightarrow Y$  and especially along the  $Y \rightarrow M$  paths in the first Brillouin zone 8 CO magnon branches are doubly degenerate, while additional degeneracies are predicted for the respective magnons in the dimer phase. For  $A' < A$  six distinct magnon branches (4 of them doubly degenerate, but other 2 with degeneration four) appear along  $\Gamma \rightarrow Y$  (while for  $A = A'$  as in Fig.5 there is a slight lifting of the extra degeneracy, being 8 branches observable), while 4 magnon branches (with degeneration four) appear along  $Y \rightarrow M$  for the dimer phase. This splitting or lifting of the dimer phase degeneracies observable in the CO phase increases proportionally with the magnitude of the antiferromagnetic in-plane  $A$  coupling (the effect disappears for  $A = 0$ ), being almost unaffected by the values of the other magnetic couplings.

The anisotropy exhibited by the magnon dispersion relations (of Figs.4 and 5) along  $\Gamma \rightarrow X$  with respect to those along  $\Gamma \rightarrow Y$  can be understood considering the spin ordering along the x and y directions (see Fig. 3). Along x, the direction of the zig-zag chains, the system can be viewed as composed by consecutive chains: one of parallel spins (e.g. up), followed by another with alternating spins, then again one of parallel spins (down), etc. While along y the system has more symmetry: it can be viewed as consecutive chains, all of them formed by alternating spins.

Apart from the qualitative differences between the magnon spectra of the CO and dimer phases which were pointed out above (mostly related to the magnitude of the antiferromagnetic in-plane coupling  $A$ ), there are also quantitative variations of the spectra related to the values of the other magnetic couplings considered. In particular, in Fig. 6 we exhibit the magnon dispersion curves for a set of parameters more suitable for the description of the dimer phase: with an intradimer ferromagnetic coupling ( $F'$ ) an order of magnitude larger than the interdimer ferromagnetic coupling ( $F$ ). This corresponds to the large estimated values ( $t \sim 100$  meV) for the effective hopping between Mn ions in these compounds<sup>12,13</sup>. Recent estimations of the ferromagnetic interdimer exchange coupling  $F$  in these compounds consider it to be of the order of 10 meV<sup>13</sup>. For strong intradimer ferromagnetic coupling as in Fig. 6, a large energy gap would then separate the magnons between higher (lying approximately around 0.1eV) and lower (around 0-0.01eV) energy modes, being the latter possibly the only ones easier to probe experimentally.

Summarizing, we have calculated the magnetic excitations to be expected for the charge ordered and the dimer phases which have been proposed for the CE magnetic structure of the half-doped manganites. We predict qualitative

differences between the magnons related to specific exchange couplings, which should allow to distinguish between these two phases in neutron scattering experiments. Not only are there lifted degeneracies in the CO phase along certain first Brillouin zone paths with respect to the dimer phase, but the presence of dimers with strong intradimer exchange coupling should result in a smaller number of magnons being detected by the experiments at low energies, while a larger number of magnetic excitations should be easily detected if the charge-ordered phase was the one being measured.

## ACKNOWLEDGEMENTS

We wish to acknowledge discussions with J.Rodríguez-Carvajal. B.A. and C.I.V. are members of the Carrera del Investigador Científico of CONICET (Consejo Nacional de Investigaciones Científicas y Técnicas, Argentina). B.A. is a researcher of C.N.E.A. (Comisión Nacional de Energía Atómica, Argentina).

- <sup>1</sup> H. Kuwahara, and Y. Tokura, in *Colossal Magnetoresistance, Charge ordering and Related Properties of Manganese Oxides*, edited by C.N.R. Rao and B. Raveau (World Scientific, Singapore, 1998); C.N.R. Rao, A. Arulraj, P.N. Santosh, and A.K. Cheetham, *Chem. Mater.* **10**, 2714 (1998).
- <sup>2</sup> E.O. Wollan, and W.C. Koehler, *Phys. Rev.* **100**, 545 (1955).
- <sup>3</sup> J. Kanamori, *J.Chem.Phys.Solids* **10**, 87(1959); J.B. Goodenough, *Magnetism and the Chemical Bond* (Interscience Publ., New York, 1963); P.W. Anderson, in *Magnetism*, Vol.I, eds. G.T.Rado and H.Suhl (Academic Press, New York, 1963).
- <sup>4</sup> J. B. Goodenough, *Phys. Rev.* **100**, 564 (1955).
- <sup>5</sup> A. Daoud-Aladine, J. Rodríguez-Carvajal, L. Pisard-Godart, M. T. Fernandez Díaz, and A. Revcolevschi, *Phys. Rev. Lett.* **89**, 97205 (2002).
- <sup>6</sup> J. García, M.C. Sánchez, G. Subias, and J.Blasco, *J. Phys. Condens. Matter* **13**, 3229 (2001).
- <sup>7</sup> D. García, K. Hallberg, C. Batista, M. Avignon, and B. Alascio, *Phys. Rev. Lett.* **85**, 3720 (2000).
- <sup>8</sup> H. Aliaga, B. Normand, K. Hallberg, M. Avignon, and B. Alascio, *Phys. Rev. B* **74**, 24422 (2001).
- <sup>9</sup> J.L. Alonso, J.A. Capitán, L. Fernández, F. Guinea, and V. Martín-Mayor, *Phys. Rev. B* **64**, 54408 (2001).
- <sup>10</sup> F. Rivadulla, E. Winkler, J. S. Zhou, and J. B. Goodenough, *Phys. Rev. B* **66**, 174432 (2002).
- <sup>11</sup> T. Holstein, and H. Primakoff, *Phys. Rev.* **58**, 1098 (1940); and e.g.see also: C. Kittel, *Quantum Theory of Solids* (Wiley, New York, 1963).
- <sup>12</sup> R. Allub, and B. Alascio, *Phys. Rev. B* **55**, 1 (1997).
- <sup>13</sup> G. Zheng, and C.H. Patterson, *cond-mat/0302622* preprint (2003).

Fig. 1. Schematic picture of the Mn<sup>3+</sup>/Mn<sup>4+</sup> charge ( +orbital) ordered (CO) scenario for half-doped manganites in the CE magnetic structure. Large arrows denote  $S = 2$  ( Mn<sup>3+</sup>) spins, while small arrows  $S = 1.5$  ( Mn<sup>4+</sup>) spins. I and II are coplanar ferromagnetic zig-zag chains, chain III is directly below I on a consecutive plane.

Fig. 2. Schematic picture of the dimer phase for half-doped manganites in the CE structure. All spins correspond to Mn ions with an intermediate valence of  $\sim 3.5$ . Thick dashed lines indicate dimers.

Fig. 3. Schematic plot of the three-dimensional 16-spin unit cell used ( Bravais lattice parameters:  $a_x = a_y = \sqrt{8}a_0$ ,  $a_z = 2c$ ). Magnetic couplings between nearest neighbour spins: ferromagnetic “intradimer” F’ (thick dashes) and “interdimer” F (solid line) along the zig-zag chains (F’=F, in CO phase), antiferromagnetic interchain A for coplanar spins (e.g. spin 9 on chain I and 14 on II) and interplane A’, for spins on chains in consecutive planes (e.g. spin 9 on chain I and 1 on III).

Fig. 4. Magnetic excitations for the charge ordered (CO) phase, along 8 paths throughout the first Brillouin zone.  $F$  is taken as the energy unit. Parameters:  $F' = F = 1$ ;  $A = 1 = A'$ ;  $S_1 = 1.3$ ,  $S_2 = 1$ ;  $c/a_0 = 1$ .

Fig. 5. Magnetic excitations for the dimer phase, along 8 paths throughout the first Brillouin zone. Parameters:  $F' = 2$ ,  $F = 1$ ;  $A = 1 = A'$ ;  $S_1 = S_2 = 1$ ;  $c/a_0 = 1$ .

Fig. 6. Magnetic excitations for the dimers phase, along 8 paths throughout the first Brillouin zone. For parameters:  $F' = 10$ ,  $F = 1$ ;  $A = 1 = A'$ ;  $S_1 = S_2 = 1$ ;  $c/a_0 = 1$ .

Fig. 1 – C.I. Ventura – PRB

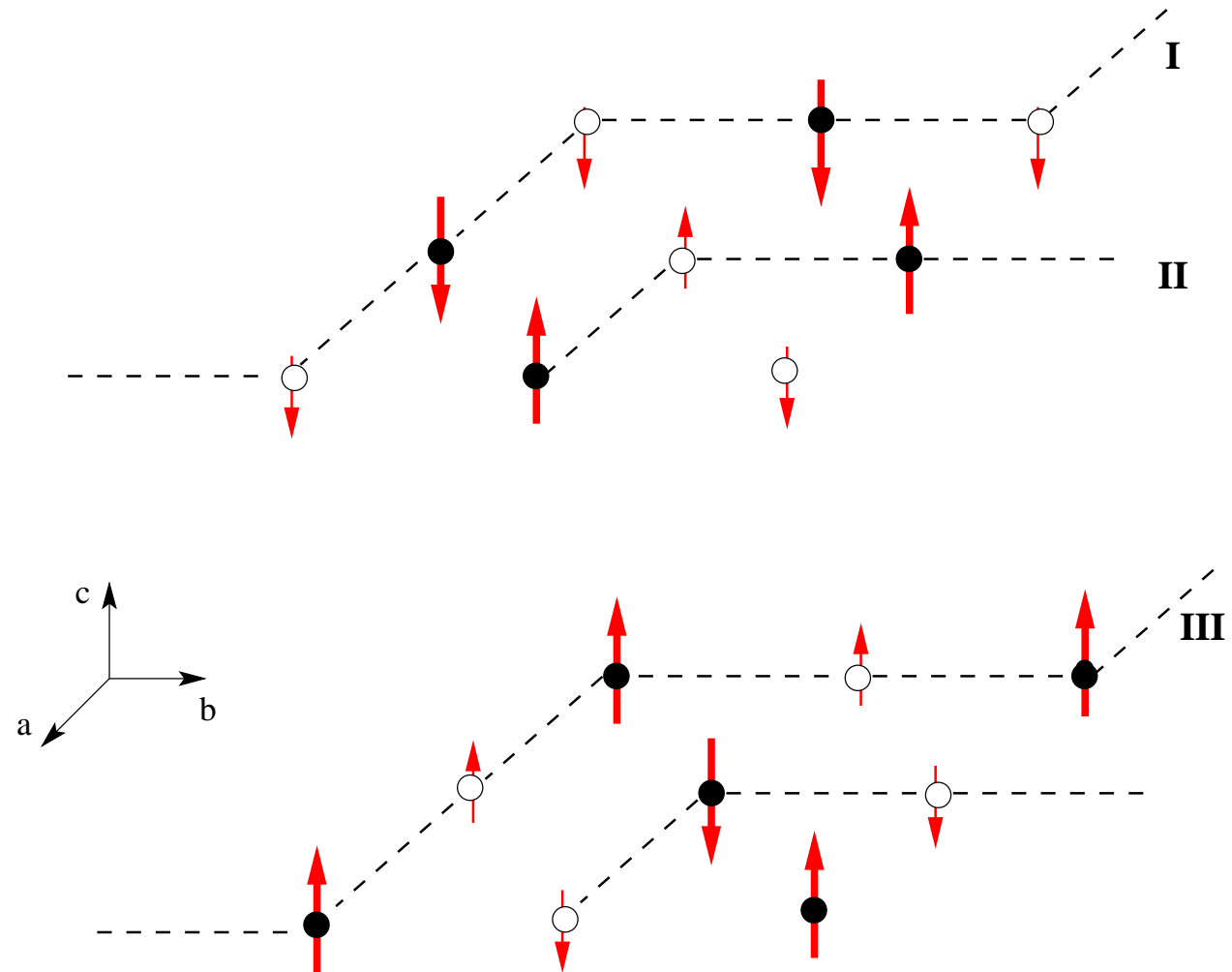


Fig. 2 – C.I. Ventura – PRB

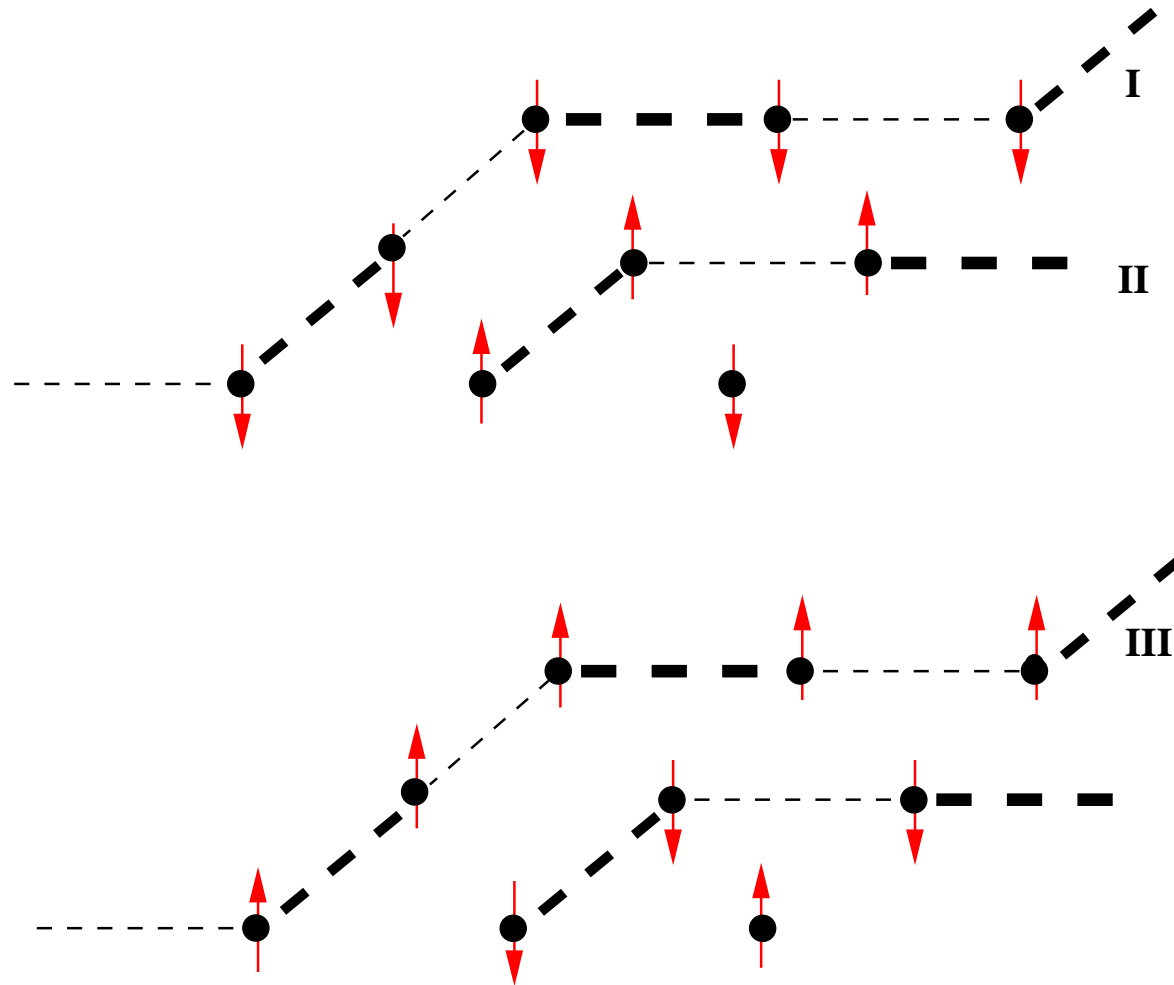


Fig. 3 – C.I. Ventura – PRB

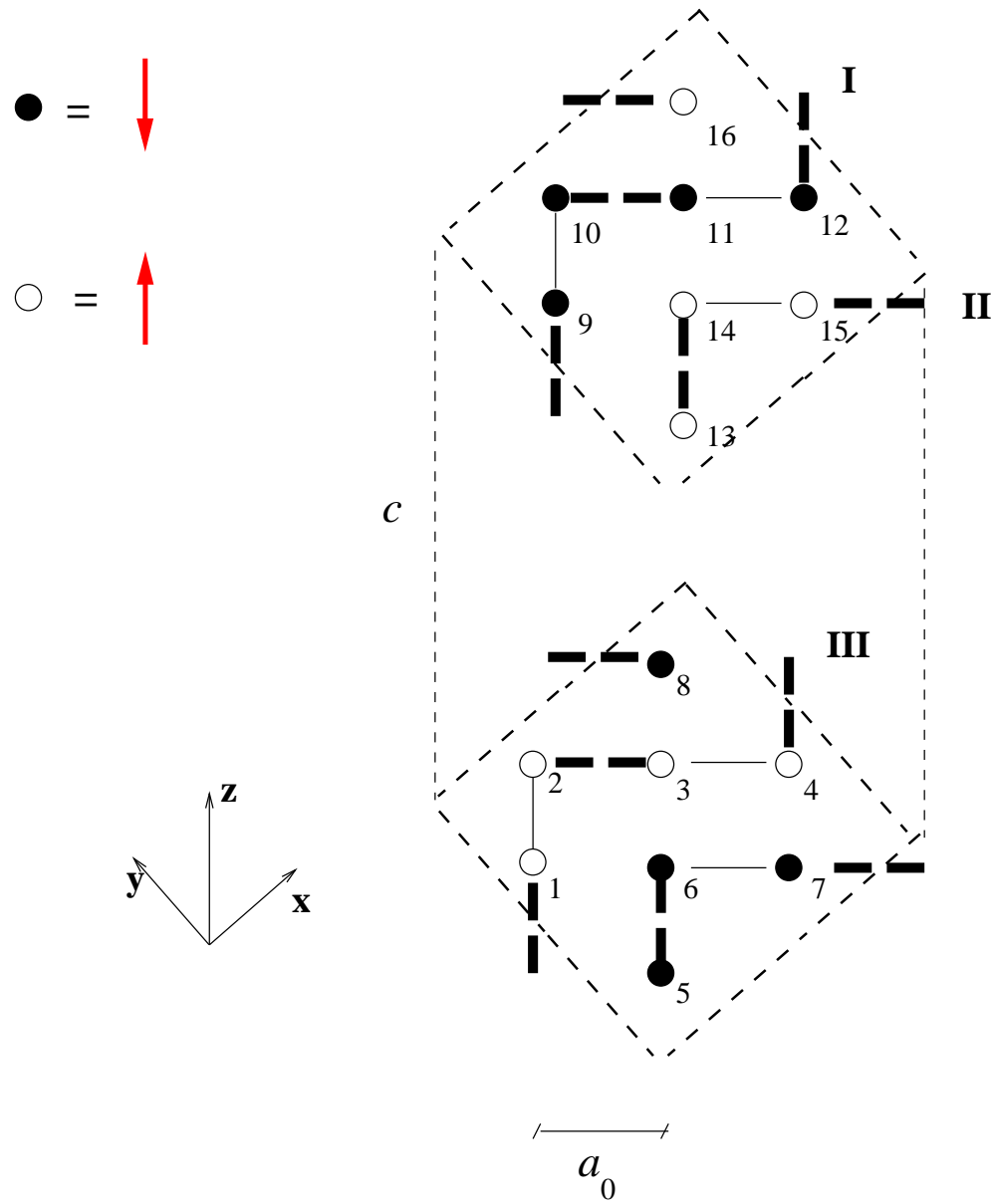




Fig. 4 - C.I. Ventura - PRB

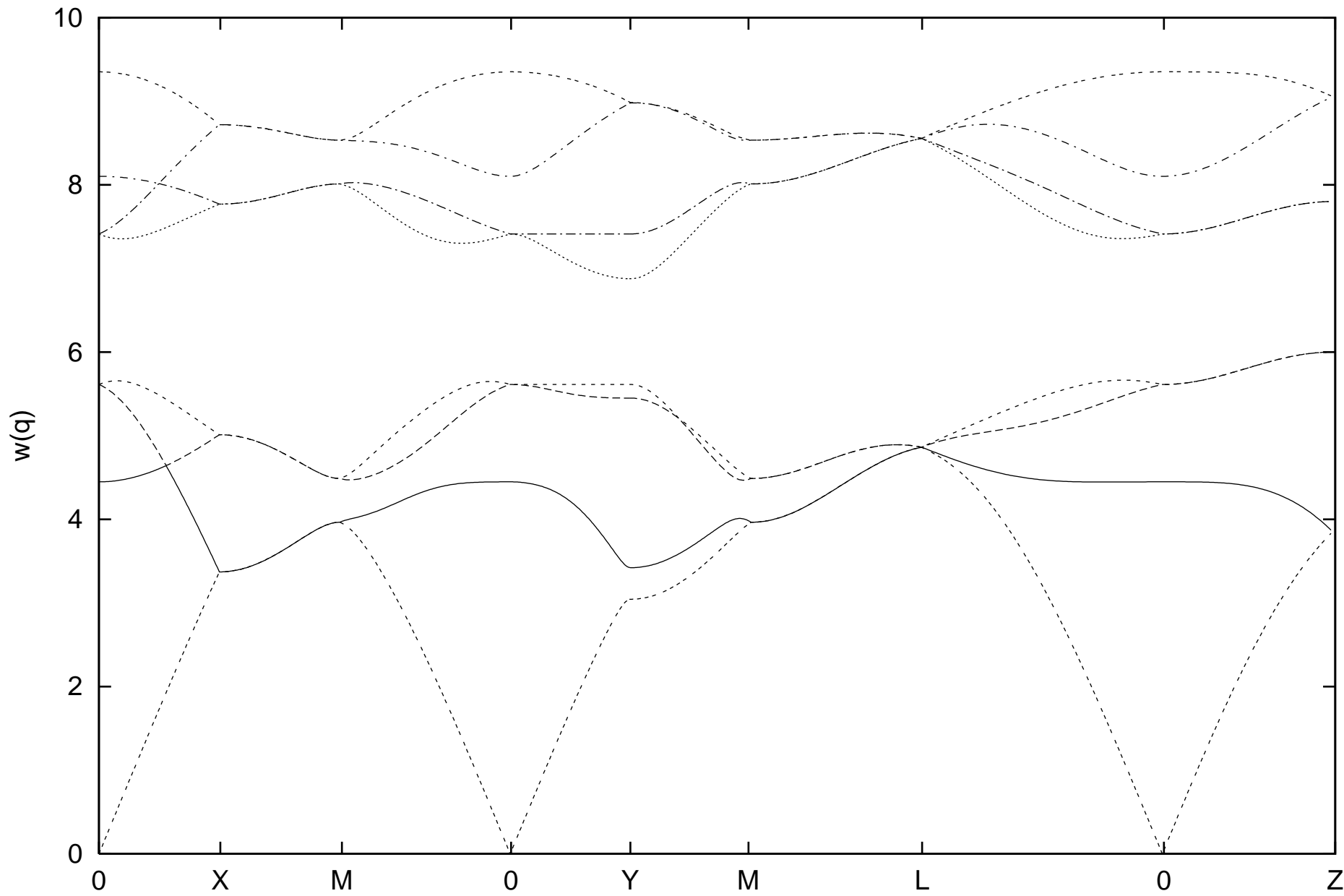


Fig. 5 - C.I. Ventura - PRB

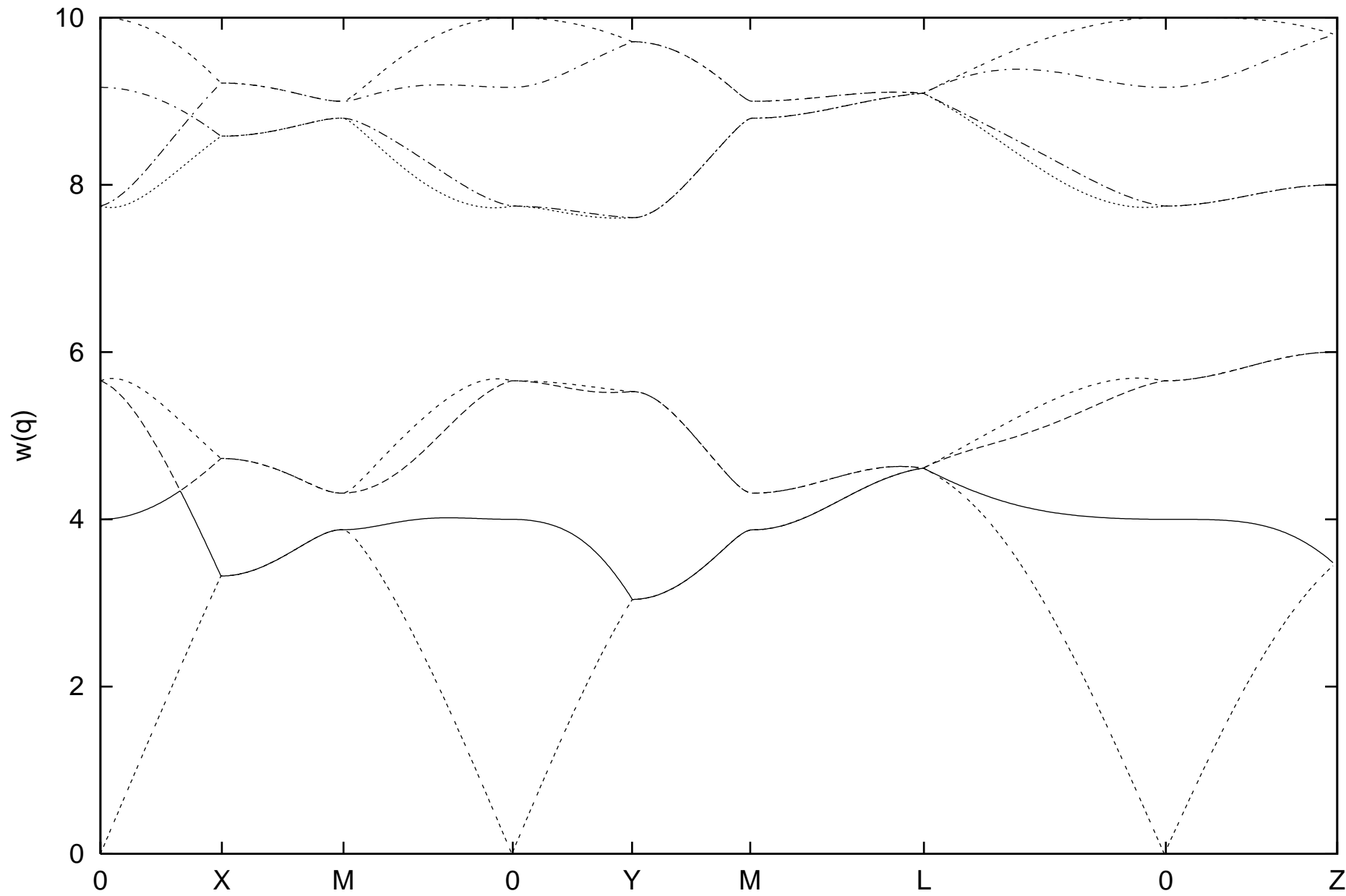


Fig. 6 - C.I. Ventura - PRB

